IET Electrical Systems in Transportation

Research Article

IET Journals
The Institution of Engineering and Technology

Power optimisation scheme of induction motor using FLC for electric vehicle

ISSN 2042-9738
Received on 18th November 2019
Revised 14th March 2020
Accepted on 3rd April 2020
E-First on 21st July 2020
doi: 10.1049/iet-est.2019.0151
www.ietdl.org

Rasha Kassem[1] ✉, Khairy Sayed[2], Ahmed Kassem[2], Ramadan Mostafa[3]

[1]*Electrical Engineering Department, Faculty of Industrial Education, Sohag University, Sohag, Egypt*
[2]*Electrical Engineering Department, Faculty of Engineering, Sohag University, Sohag, Egypt*
[3]*Process Control Technology Department, Faculty of Industrial Education, Beni-Suef University, Beni-Suef, Egypt*
✉ *E-mail: Rashaeginer@yahoo.com*

Abstract: In electric vehicles (EVs) and hybrid EVs, energy efficiency is essential where the energy storage is limited. Adding to its high stability and low cost, the induction motor efficiency improves with loss minimisation. Also, it can consume more power than the actual need to perform its working when it is operating in less than full load condition. This study proposes a control strategy based on the fuzzy logic control (FLC) for EV applications. FLC controller can improve the starting current amplitude and saves more power. Through the MATLAB/SIMULINK software package, the performance of this control was verified through simulation. As compared with the conventional proportional integral derivative controller, the simulation schemes show good, high-performance results in time-domain response and rapid rejection of system-affected disturbance. Therefore, the core losses of the induction motor are greatly reduced, and in this way improves the efficiency of the driving system. Finally, the suggested control system is validated by the experimental results obtained in the authors' laboratory, which are in good agreement with the simulation results.

1 Introduction

The weighty consumption of fossil fuels continues to rise significantly, particularly in the last few decades which led to increasing the concentration of CO_2 in the atmosphere. Worries about climate change and rising sea levels caused by global warming are becoming more serious and global efforts to reduce carbon dioxide have become a urgent need. A significant improvement in the fuel efficiency of vehicles is essential, as the transport area accounts for about 20% of total carbon dioxide emissions [1–6]. Electric vehicles (EVs) have several advantages because they are more efficient, more environmentally friendly, quiet, and commonly reduce the energy dependence [7]. The choice of the electric machine has an important effect on the efficiency and cost of the drive. However, electric machines are an essential part of any drive such as those that can be integrated into EVs and hybrid EVs [8]. The synchronous motors and induction motors (IMs) are the main types of machines that can be utilised in EVs [9]. The EV-drive motor should feature the following propulsion [7, 10–12]:

(i) high torque density to give enough driving force during startup, climbing and acceleration;
(ii) high efficiency to increase driving distance;
(iii) good flow regulating ability to extend the static power speed range.

The IM is more common to use for the traction drive and is the best candidate for EVs because of its strength, lower cost and low maintenance need [13–16], but its' losses are significantly higher in the EV application [17, 18] and this leads to a drop in the machine efficiency. The most restrictive barriers to accepting such vehicles in the transport system are low energy density, heavier weight, longer charging times and longer battery life [19]. Thus, the optimal use of energy is critical to the operation of EVs [20–22]. Due to their effectiveness and simplicity of implementation, it is generally believed that proportional integral derivative (PID) control which is used in many industrial drives is one of the most common units. Also, PID controllers are involved in most existing control loops and are used in industrial applications [23, 24]. While changing the operation conditions, significant performance degradation may occur due to the obsolescence of components or alteration of the working environment [25]. Due to the uncertainty and difficulty of modelling the precise analytical model of a controlled system, better performance can be provided by using intelligent control techniques such as fuzzy logic control (FLC) [26–28].

The FLC system offers many rules of strategy that use linguistic tags more simply. This approach has been used in much other energy demand management work in EVs [7]. FLC is a model-free approach, it does not require a mathematical model of a controlled system [28, 29]. Therefore, for improving the performance of the EV traction, the FLC system controller should be designed with adaptive properties when the system enters areas with fixed errors. Finding suitable compromises between fast ascending time, minimum steady-state error, and minimum overshoot are other trends in FLC [30].

However, reducing steady-state losses is the point of interest in the existing design methods [31, 32]. High and excessive current peak losses in the machine can occur during transit with varying flow links when conventional induction machines are designed for high stability efficiency. Therefore, this paper focuses on the losses of transient machines that occur during the very dynamic driving cycle normally encountered by the EV traction motor drive.

In the literature, many different control structures have been provided for EV applications. These include simple linear techniques such as field oriented control [8, 33], direct torque control [34, 35], and sliding mode control [36]. Reduce secondary winding harmonic losses by using the finite element method [17], using the model reference adaptive system with an optimised base power scheme known as the golden section method [33]. Using search controller (SC) which is based on adaptive quadratic interpolation to optimise the loss of IM drive [20], and also using the slip control that is carried out through a fuzzy controller with nine rules, taking speed error change as input, to produced frequency.

In this work, an FLC-based method is proposed for EV applications. A comparison between each of the controllers (PID and FLC) is then presented based on their impact on IM performance. The main contributions resulting from this work can

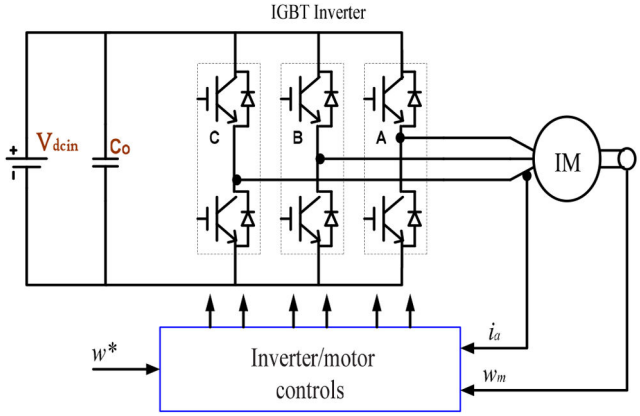

Fig. 1 *EV drive with an IM*

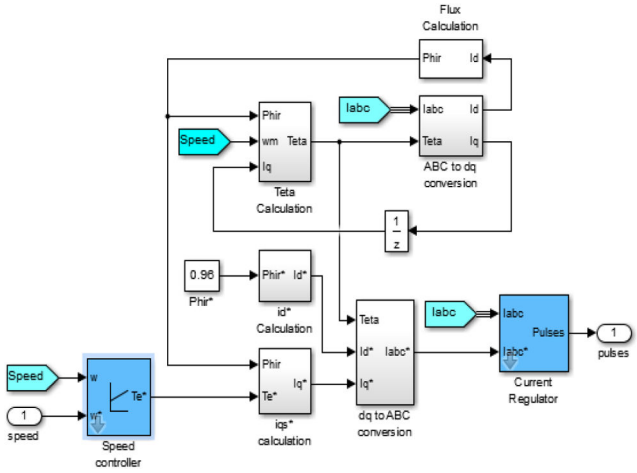

Fig. 2 *Control system of IM*

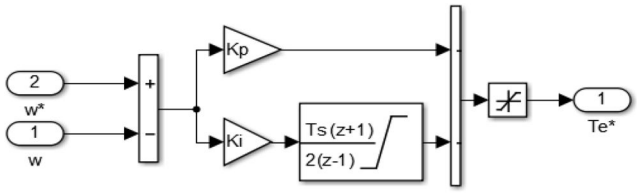

Fig. 3 *Block diagram of the conventional PID controller*

be summarised as follows: the main issue is to minimise the cost of the drive life cycle, at estimated speeds and above, and efficiency is an indicator of the cost of energy. The efficiency of the inverter is affected by the total drive efficiency.

The rest of the paper is organised as follows: In Section 2, the circuit description is presented, and the control principle is given in Section 3. Power losses calculations and efficiency of IM drive are analysed in Section 4. In Section 5, the simulation results and in Section 6, experimental results are carried out and presented and finally the conclusion is given in Section 7.

2 Circuit description

As shown in Fig. 1, battery EV is electrically operated vehicle alone and consists of three main parts: firstly, an electric motor system, often there is only one electrical machine, usually, a three-phase AC. Connected to the wheel via the gearbox and differential. Secondly, a battery that acts as a power store, and the energy is stored chemically in the battery, which is plugged into the device by an electronic DC/AC power adapter accompanied by the control system. Lastly, the three-phase frequency and voltage control system applied to the electric machine, depending on the current driver's request, which is connected by the accelerator pedal and/or brake pedal.

In Fig. 1 the three-phase electric machine provides traction power for wheels. The differential with gear ratio for high-speed adjustment of the electric motor shaft to the low speed of the wheels will provide torque for the left and right wheels. The speed of the machine is controlled by an inverter that converts the battery voltage DC to the three-phase AC voltage. It is important to include losses from components when analysing the power consumption of an EV that is not part of the power chain from the grid to the wheels. To push the EV system into the required operation, our commitment is to create suitable controllers for feedback. The inadequately adaptable, flexible and powerful controller can be implemented by adopting FLC techniques for EVs applications.

3 Control principle

3.1 Conventional PID control

A classical PID controller is introduced in the first design approach for applying to an indirect field-oriented IM order to control its speed and also starting situation is investigated. As illustrated in Fig. 2 the proposed control system includes a (direct–quadrature–zero) conversion equations, and a phase-locked loop algorithm that synchronises with the utility current regulator. The phase currents (ia, ib, ic) are converted from a–b–c coordinates to a d–q frame. The components of d–q can be described using the following conversions:

$$\begin{bmatrix} i_d \\ i_q \end{bmatrix} = \sqrt{\frac{2}{3}} \begin{bmatrix} \sin(\omega t) & \sin\left(\omega t - \frac{2\pi}{3}\right) & \sin\left(\omega t + \frac{2\pi}{3}\right) \\ \cos(\omega t) & \cos\left(\omega t - \frac{2\pi}{3}\right) & \cos\left(\omega t + \frac{2\pi}{3}\right) \end{bmatrix} \times \begin{bmatrix} i_{sa} \\ i_{sb} \\ i_{sc} \end{bmatrix} \quad (1)$$

The active and reactive power calculated now includes oscillation and average components. However, two outer PID control loops are utilised to acquire the average components to the outputs of the active power and reactive power. A block diagram of the conventional PID control is given in Fig. 3. This PID produces active current reference (i_d*) and reactive current reference (i_q*), as given in the following conversions:

$$i_d^* = k_{\mathrm{p}}(P_{\mathrm{ref}} - P) + k_{\mathrm{i}} \int (P_{\mathrm{ref}} - P)\,\mathrm{d}t \quad (2)$$

$$i_q^* = k_{\mathrm{p}}(Q_{\mathrm{ref}} - Q) + k_{\mathrm{i}} \int (Q_{\mathrm{ref}} - Q)\,\mathrm{d}t \quad (3)$$

where k_{p} is the proportional constant and k_{i} is the basic constant, for the PID controllers used. P_{ref} is the charging power reference and Q_{ref} is the reference value of the reactive power required by the AC source.

The control is designed by integrating the inner current loop and the outer voltage loop. When comparing the current reference with the actual current in the outer loop produces the current reference, and it is used to control the inner loop. Consequently, the internal PID loops are generated by comparing the measured line currents obtained using the Park conversion. The results (e_d and e_q) are first summarised by the disengagement conditions and then normalised by the DC voltage to obtain the operating ratios in the d–q coordinates as follows:

$$\begin{bmatrix} d_d \\ d_q \end{bmatrix} = \frac{1}{V_{\mathrm{dc}}} \begin{bmatrix} e_d + v_d + 3\omega L \times i_q \\ e_q + v_q - 3\omega L \times i_d \end{bmatrix} \quad (4)$$

Inverse matrix transformation can be used to obtain the duty ratios in (a–b–c) frame coordinates, which can be expressed as follows:

$$\begin{bmatrix} D_a \\ D_b \\ D_c \end{bmatrix} = \sqrt{\frac{2}{3}} \begin{bmatrix} \sin(\omega t) & \cos(\omega t) \\ \sin\left(\omega t - \frac{2\pi}{3}\right) & \cos\left(\omega t - \frac{2\pi}{3}\right) \\ \sin\left(\omega t + \frac{2\pi}{3}\right) & \cos\left(\omega t + \frac{2\pi}{3}\right) \end{bmatrix} \times \begin{bmatrix} d_d \\ d_q \end{bmatrix} \quad (5)$$

3.2 Description of suggested FLC

Due to the non-linear characteristics of AC motors, especially the squirrel cage induction motor (SCIM), controlling this problem remains a difficult problem because many factors (mainly rotor resistances) vary with operating conditions. Therefore, traditional control technology (PID) must be changed using the effective intelligent FLC [37] for EV applications. The most important considerations in the design of any fuzzy system are:

(i) generation of fuzzy rules for some control issues, which are created by experts in the area;
(ii) selecting the membership functions and adjusting;
(iii) selecting the scaling factors.

In the second design approach, the basic FLC was developed for EV applications, which serve as a type of variable structure control unit that is well established for stability and durability. Fig. 4 shows a typical FLC.

A new approach to improve adjustable speed drives voltage, frequency, and current control is provided using the mathematical technique called fuzzy logic. It can be applied to problems that make non-linearity and its dynamic nature intractable by conventional control methods in for EV applications. Motor control has all the characteristics of this type of problem.

3.3 Speed control using FLC

Two input variables for FLC in the case of motor speed control are needed, which are the motor speed error (*we*) and its derivative that represents the speed variation error (Δ*we*). Speed error and speed variation error could be described as follows:

$$we = w^*_{\text{ref}} - w_{\text{act}} \quad (6)$$

where w^*_{ref} and w_{act} denote the reference motor speed and the actual/or measured motor speed, respectively:

$$\frac{\mathrm{d}we}{\mathrm{d}t} = \frac{\Delta we}{T_s} \quad (7)$$

The controller output is the incremental change of the control signal Δ*u*. The control signal can be obtained by

$$\Delta u = \Delta t^*_e = k_1 \cdot we + k_2 \cdot \Delta we \quad (8)$$

where k_1 and k_2 represent the current and previous states of the system, respectively. The universe of discourse in all membership functions of the controller inputs, i.e., *we* and Δ*we*, and the output, i.e. Δ*u*, are defined on the normalised domain [−1, 1], as shown in Fig. 5.

Five membership function (MF) for inputs and five MF for output fuzzy sets have been used to partition the fuzzy logic membership functions as shown in Fig. 5.

To relate two input variables to one output variable, a Mamdani fuzzy inference system is used in this system. The two input variables are the error (*we*), which are the differences between the desired (set-point) and measured speed, and the change of error (Δ*we*). The scaling factors *Ge*, *Gde*, and *Gu*, in Fig. 4, which perform the normalisation process and denormalisation of the specific variables of a conventional control gain. When *Ge*, *Gde*, and *Gu* are the error measurement, error variation, and FLC output factors respectively, the value of these measurement factors is based on the initial error. Limited models are used to reduce the error and variation in the error between (1, −1) the input and output functions of the FLC as shown in Fig. 5, while the FLC rules are

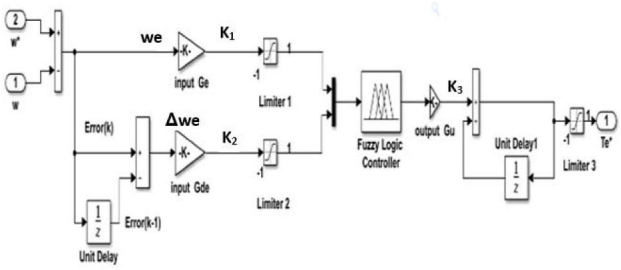

Fig. 4 *Detailed construction of the fuzzy controller*

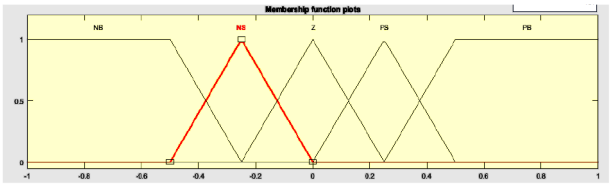

Fig. 5 *Membership function of FLC (we), (Δwe), (Δu)*

Table 1 Rules of the FLC

Δ*we*	*we*				
	NB	NS	Z	PS	PB
NB	NB	NB	NS	NS	Z
NS	NB	NS	NS	Z	PS
Z	NS	NS	Z	PS	PS
PS	NS	Z	PS	PS	PB
PB	Z	PS	PS	PB	PB

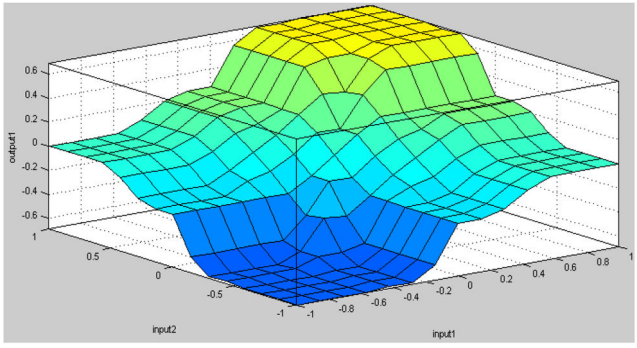

Fig. 6 *Crisp in./out. map*

registered in Table 1. This feature gives a hint of using the interpolation of the basic table of rules to create a more precise continuous control rule than simply taking NB, NS, Z, PS, and PB stand for negative big, negative small, zero, positive small, and positive big, respectively. Here except for two obscure groups at the outer ends (trapezoidal MFs are chosen), symmetrical triangles are selected with an equal base and 50% overlap with adjacent MFs.

As shown in Table 1, there are five fuzzy subsets for each variable, which gives 25 possible rules, where the typical rule is: 'If *e* is NB and *de* is PB Then *u* is *Z*'.

Speed correction control is a need because the motor speed and output power are altered by the perturbation approach. The motor's output rotor speed should be maintained as constant as possible. The input/output mapping of the FLC is shown in Fig. 6.

Smooth torque and improvement in the system performance can be produced for EV applications by using this fuzzy controller in the outer loop by taking the speed error and variation of error as input signals to create the equivalent control terms.

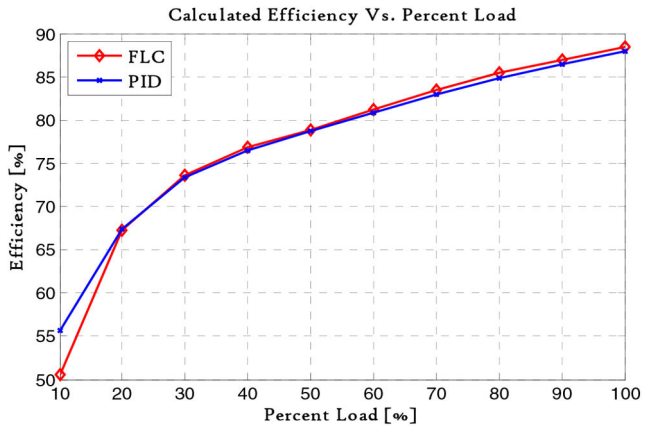

Fig. 7 *Efficiency of the IM drive using PID versus FLC*

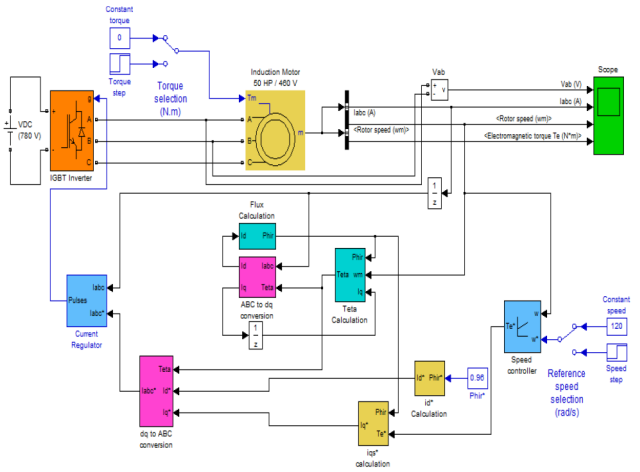

Fig. 8 *MATLAB model of three-phase IM*

4 Power loss calculations and efficiency of induction motor drive

The following power losses of the proposed control scheme at full load for a worst-case scenario are estimated to verify the measured efficiency.

4.1 Parameters

This section shows the entire given and calculated parameters in Table 2. The parameters come from the typical values listed in the datasheets. Next, some calculated parameters will be shown, and the stray losses are negligible in [38].

4.2 Input power losses

Three-phase IM is drawing 62.6 A at 0.85 PF lagging using PID, and 60 A at 0.85 PF lagging using FLC. The input power losses can be estimated as

$$P_{\text{In}} = \sqrt{3} \times V_{\text{L}} I_{\text{L}} \cos\theta = 3 \times V_{\text{ph}} I_{\text{ph}} \cos\theta \tag{9}$$

4.3 Air-gap power losses

The stator copper losses are 2 kW, and the core losses are 1.8 kW, which is taken into consideration. The air-gap power losses can be estimated as

$$\begin{aligned} P_{\text{AG}} &= P_{\text{In}} - (P_{\text{SCL}} + P_{\text{Core}}) \\ &= P_{\text{Conv}} + P_{\text{RCL}} = 3I_2^2 \frac{R_2}{S} = \frac{P_{\text{RCL}}}{S} \end{aligned} \tag{10}$$

Table 2 Given and calculated parameters

Item	Symbol	Value
voltage (line-to-line)	V_{L}	460 V
frequency	F	60 Hz
number of poles	P	4
power factor	PF	0.85 lagging
three-phase IM is drawing (PID)	I_{L}	62.6 A
three-phase IM is drawing (FLC)	I_{L}	60 A
stator copper losses (PID)	P_{SCL}	2 kW
stator copper losses (FLC)	P_{SCL}	1.8 kW
rotor copper losses (PID)	P_{RCL}	700 W
rotor copper losses (FLC)	P_{RCL}	500 W
core losses	PC_{ore}	1.8 kW
friction and windage losses	$P_{\text{F\&W}}$	600 W

Table 3 Results of power losses analysis under full load and efficiency estimation of IM drive using PID and FLC

Item	Power losses calculation	PID	FLC
input power	$P_{\text{In}} = \sqrt{3} \times V_{\text{L}} I_{\text{L}} \cos\theta = 3 \times V_{\text{ph}} I_{\text{ph}} \cos\theta$	42.395 kW	40.634 kW
air-gap power losses	$P_{\text{AG}} = P_{\text{In}} - (P_{\text{SCL}} + P_{\text{Core}})$	38.595 kW	37.034 kW
converted power losses	$P_{\text{Conv}} = P_{\text{AG}} - P_{\text{RCL}}$	37.895 kW	36.534 kW
output power	$P_{\text{out}} = P_{\text{Conv}} - (P_{\text{f\&w}} + P_{\text{stray}})$	37.295 kW	35.934 kW
efficiency	$\eta = \frac{P_{\text{out}}}{P_{\text{in}}} \times 100$	87.97%	88.43%

4.4 Converted power losses

To calculated power converted, the only rotor copper losses are 700 W, is that taken into consideration. The converted power losses can be estimated as

$$\begin{aligned} P_{\text{Conv}} &= P_{\text{AG}} - P_{\text{RCL}} \\ &= 3I_2^2 \frac{R_2(1-S)}{S} = \frac{P_{\text{RCL}}(1-S)}{S} \end{aligned} \tag{11}$$

$$P_{\text{Conv}} = (1-S) P_{\text{AG}} \tag{12}$$

4.5 Output power losses

The calculation assumes that stray losses are negligible and thus the friction and windage losses are 600 W, which is that taken into respect. The output power losses can be estimated as shown in Table 3

$$P_{\text{Out}} = P_{\text{Conv}} - (P_{f+w} + P_{stray}) \tag{13}$$

Fig. 7 shows the efficiency of the IM drive versus per cent load. From this figure, the energy efficiency increases when the IM runs at optimal performance. By comparison between the results obtained by the controller tuned using some known tuning rules and the results obtained by the suggested rules, a worthier performance is achieved by the proposed.

5 Simulation results

Simulink and power sum toolboxes of MATLAB software are used in the simulation, where two cases have been considered as shown in Fig. 8. In the first case study, a 50 hp IM is powered using a PID controller. Three-phase voltage and current are measured and planned in the first 5 s of operation. Also, the probe is made in the acceleration curve and the resulting torque. In the second case, the motor itself is operated using FLC. PID controller response is

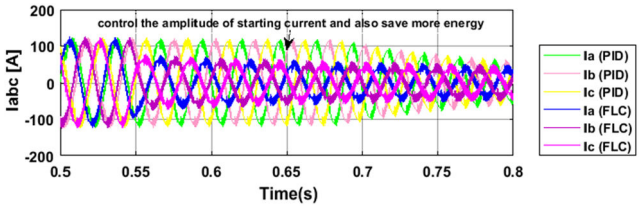

Fig. 9 *Three-phase stator current of PID and FLC models (A)*

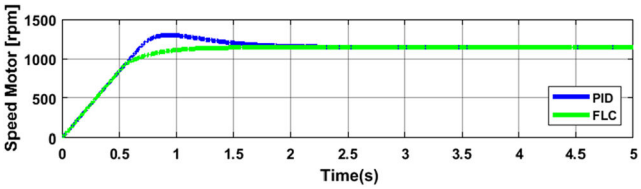

Fig. 10 *Simulation response of PID and FLC for rotor speed (rpm)*

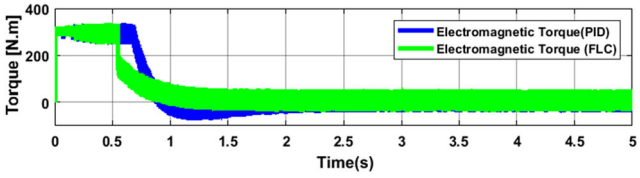

Fig. 11 *Simulation response of PID and FLC for electromagnetic torque (N m)*

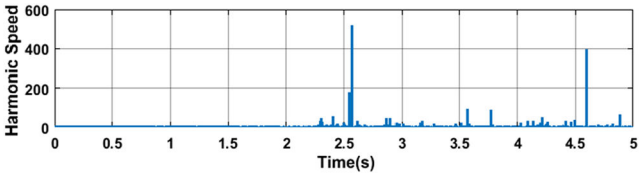

Fig. 12 *Harmonic speed waveform of the PID model*

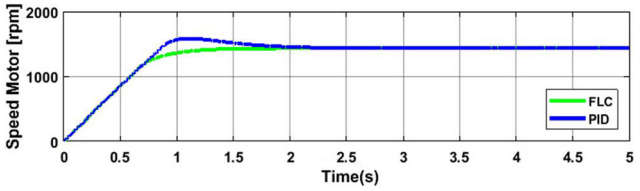

Fig. 14 *Speed response comparison for PID and FLC when the reference speed is 1432 rpm*

compared with the FLC response and the results are shown in Figs. 9–11.

From the given figures, regarding the magnitude of starting currents, an improvement has been achieved for the outputs and time response of acceleration. The phase current with the suggested method contains fewer loss components in the same order of components. This shows that the system produced actual torque smoother and reduces the speed variation [30]. Figs. 12 and 13 show the harmonic speed waveform of the PID model and the FLC model, respectively.

Several simulation tests were done using both PID and FLC to control the IM speed. The performance results of the control unit were tested by a gradual variation of the speed reference at a constant load torque as shown in Figs. 14–16. Table 4 shows a comparison between the performance of PID and FLC, in terms of peak overshoot, settling time and rising time, when the multistep speed input.

It is clear from Table 4 that except for the rise time at 1145 (rpm), FLC compared with PID response for multistep speed input provides a faster response in both settling and rise time. So FLC compared with PID showed better performance. Also, FLC showed a better ability to control the speed of the three-phase IM and

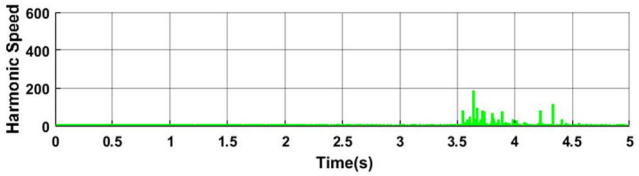

Fig. 13 *Harmonic speed waveform of the FLC model*

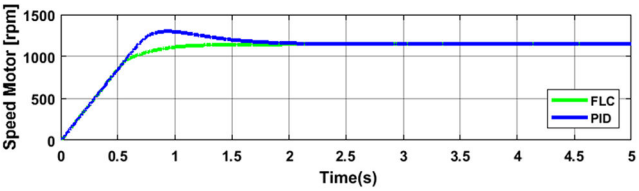

Fig. 15 *Speed response comparison for PID and FLC when the reference speed is 1145 rpm*

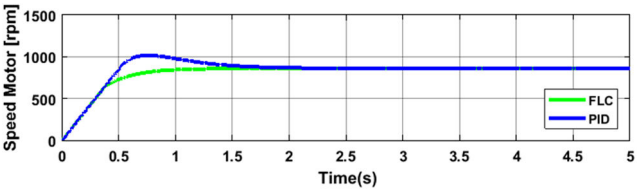

Fig. 16 *Speed response comparison for PID and FLC when the reference speed is 859 rpm*

provide an accurate and fast response with relatively no steady-state error and no overshoot.

Several simulation tests were done using both PID and FLC to control the speed of IM for EV applications. Simulations were carried out using various operating conditions such as reference speed and applied load. The performance of PID and FLC was analysed and compared. The speed response of FLC for selected reference speeds and its performance during load disturbance are shown in Figs. 17*a* and *b*.

Fig. 18 shows the results of a 20 s simulation. At time $t = 0$, the vehicle is completely stopped and the accelerator is suddenly pushed to 70%. The car starts in electrical mode until the power required by the vehicle reaches 10 kW (at $t = 0.8$ s). At the time $t = 12$ s, the brakes are pushed to 70%. This turns on the electric motor to transfer the brake energy to the battery and charge it for 4 s. At the time $t = 16$ s, the accelerator is suddenly pushed to 70% again [39].

6 Experimental results

The experimental circuit setup treated here is shown in Fig. 19. The control system is given in a block diagram in the same figure. The insulated gate bipolar transistor (IGBT) power modules CM900CU-24NF are each IGBT with reverse conducting diode in the six in one IGBT power modules is used for switches $Q_1(S_1/D_1)$, $Q_2(S_2/D_2)$ and $Q_3(S_3/D_3)$ and the upper IGBT with reverse conducting diode in the six in one IGBT modules is used ad diode while two IGBT is not in use. The obtained experimental results of the proposed FLC control scheme provide very good stability and better performance over the conventional PID controller in total harmonic distortion. Also, the experimental results were in good agreement with the simulated results.

Three-phase inverter: The inverter is very important electronical equipment, and the function of the inverter is to convert the DC signals to AC signals as shown in Fig. 20. The generated voltage of the inverter has two forms, the first form is the (AC) voltage (e.g. sine wave and square wave) and the second form is the sine modulation (modulation sine wave). The semiconductor industry is commonly used in the power devices like the inverter, MOSFET, IGBT, transistor or thyristor.

Level shifter: Level shifter IC (40109) is used to drive pulses that come from the *Arduino* controller to the inverter from the low-

Table 4 Comparison of FLC and PID performance in multistep speed response. The sampling time is $T_s = 2e^{-6}$ s

Reference speed, rpm	Rise time, s		Settling time, s		Peak overshoot, %	
	FLC	PID	FLC	PID	FLC	PID
1432	0.731	0.681	1.982	2.584	0.501	10.55
1145	0.630	0.543	1.910	2.679	0.496	13.06
859	0.547	0.402	1.868	2.419	0.489	18.45

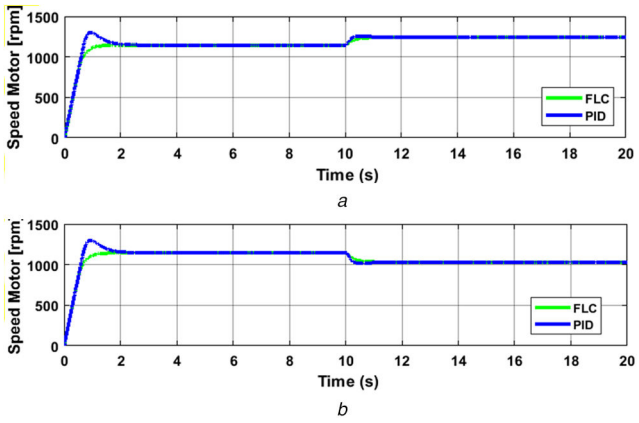

Fig. 17 *Speed response comparison for PID and FLC*
(a), ***(b)*** *IM response to speed variations ± 100 rpm during 10 s of rated load*

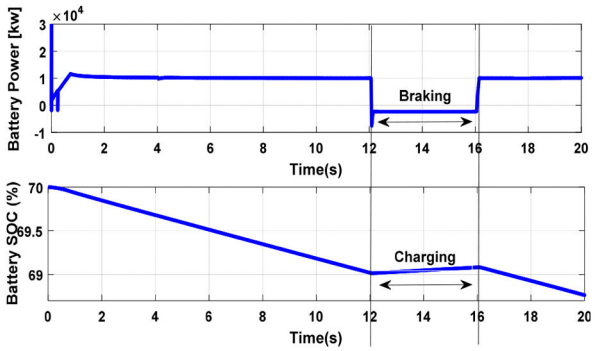

Fig. 18 *Shows battery performance during charging and discharging modes*

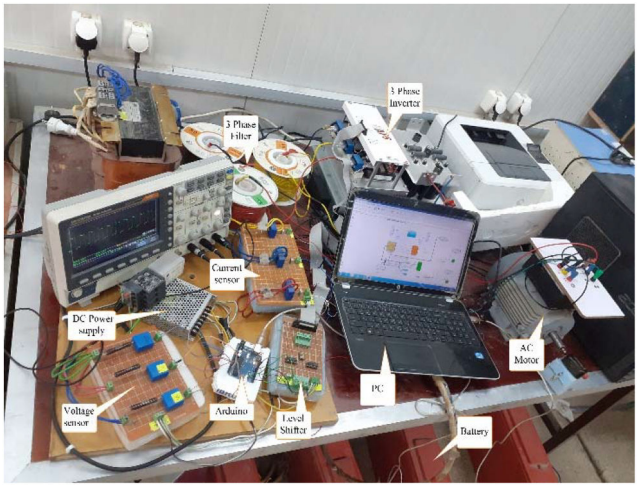

Fig. 19 *Experimental prototype of the system circuit diagram*

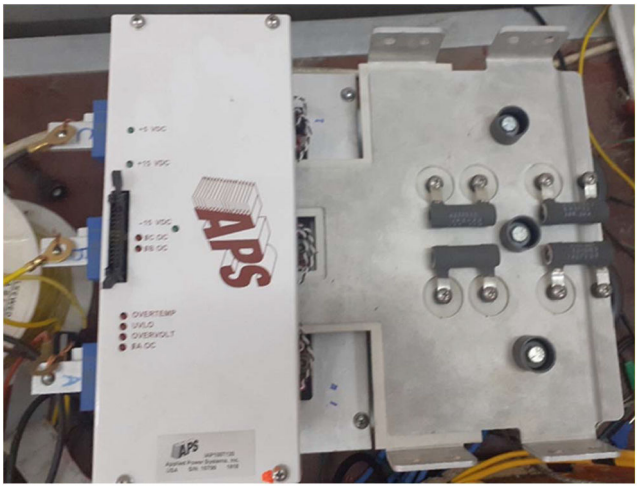

Fig. 20 *Three-phase inverter device*

level VCC (5 V) to high-Level Vo (15 V). Fig. 21 shows the design diagram of the level shifter.

Arduino: The Duemilanove board features an Atmel ATmega328 microcontroller operating at 5 V with 2 Kb of RAM, 32 Kb of flash memory for storing programs and 1 Kb of EEPROM for storing parameters. The clock speed is 16 MHz, which translates to executing about 300,000 lines of C source code per second. The board has 14 digital I/O pins and 6 analogue input pins. There is a USB connector for talking to the host computer and a DC power jack for connecting an external 6–20 V power source as shown in Fig. 22.

Voltage sensor: To estimate the voltages generated in the motor, three voltage sensors are required. The sensors used are the hall effect sensors manufactured by life energy motion (LEM). Fig. 23 shows the design diagram of the voltage sensors and how to connect them.

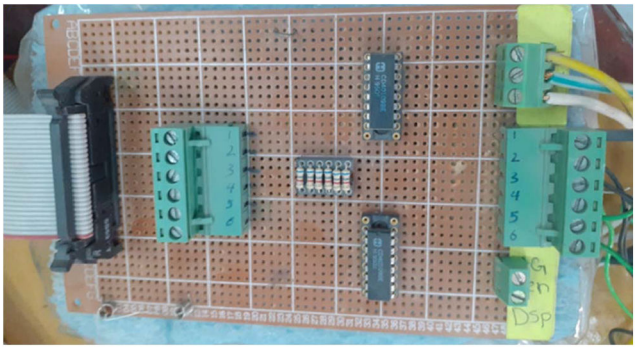

Fig. 21 *Level shifter board*

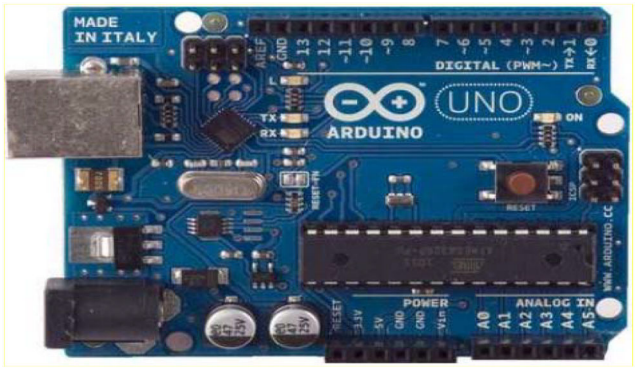

Fig. 22 *Arduino board*

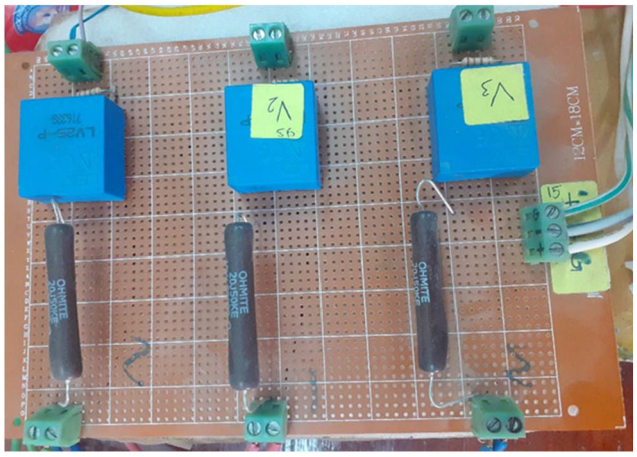

Fig. 23 *Voltage sensor board*

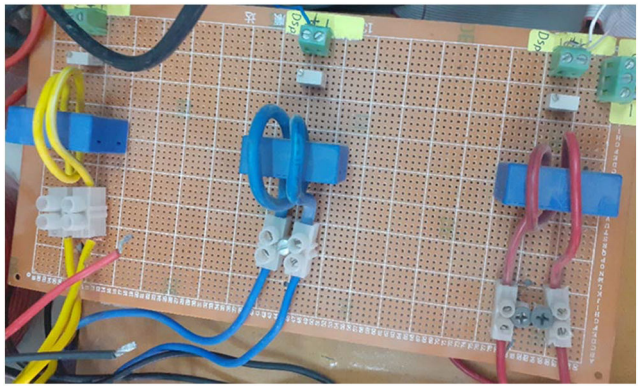

Fig. 24 *Current sensor board*

Current sensor: Three current sensors are used to measure the current injected into the motor. Each current sensor can measure up to 25 A. Sensors are hall effect sensors and are manufactured by

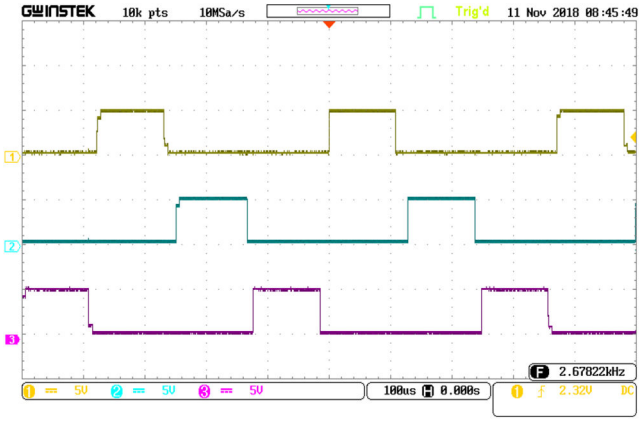

Fig. 25 *Experimental validation of the gate control signals*

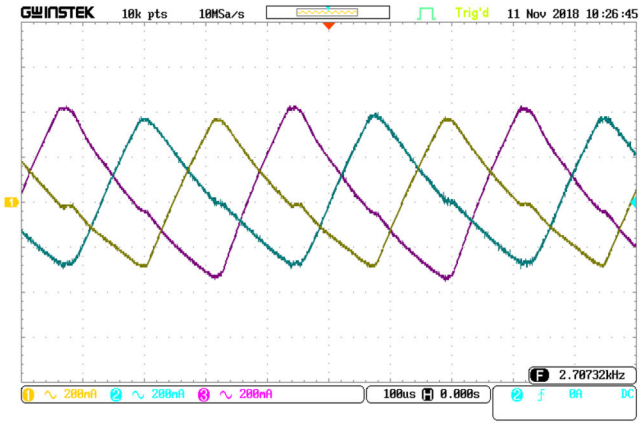

Fig. 26 *Experimental validation of the stator current of the PID model (A)*

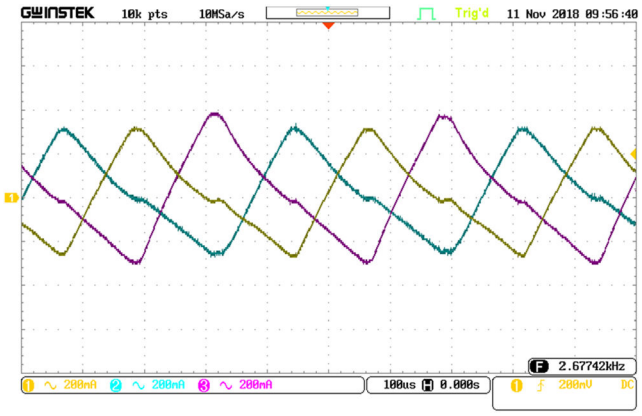

Fig. 27 *Experimental validation of the stator current of the FLC model (A)*

LEM. The circuit of the current sensor card implemented is shown in Fig. 24.

Fig. 25 shows the experimental waveforms of the gate control signal (Q_1, Q_2, Q_3). Fig. 26 shows the experimental validation of the stator current of the PID model. Fig. 27 shows an experimental validation of the stator current of the FLC model. Fig. 28 shows the experimental validation of the harmonic speed waveform of the PID model and Fig. 29 shows the experimental validation of the harmonic speed waveform of the FLC model. By analysing the total harmonic distortion (THD) in simulated and experimental results, the resulting THD was 1.198% for the PID identifier, as opposed to 0.4115% for FLC. Thus, there is a 35% increase in the fundamental output with improvement in quality (i.e. THD lower compared to PID) using the FLC. Experimental results show that when IM operates at optimal flux, the energy efficiency increases. Also, these figures show the superiority of the proposed controller in reducing the losses during drive cycles in an EV.

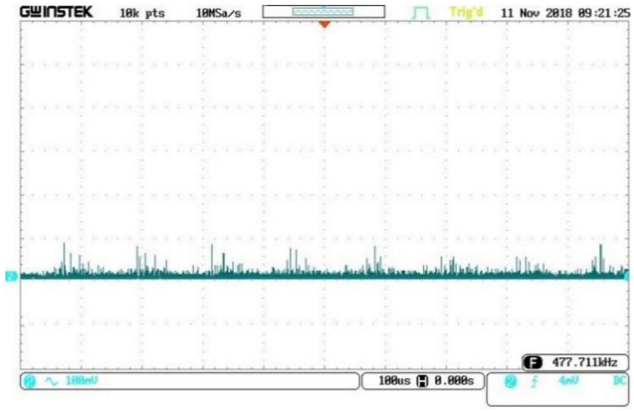

Fig. 28 *Experimental validation of the harmonic speed waveform of the PID model*

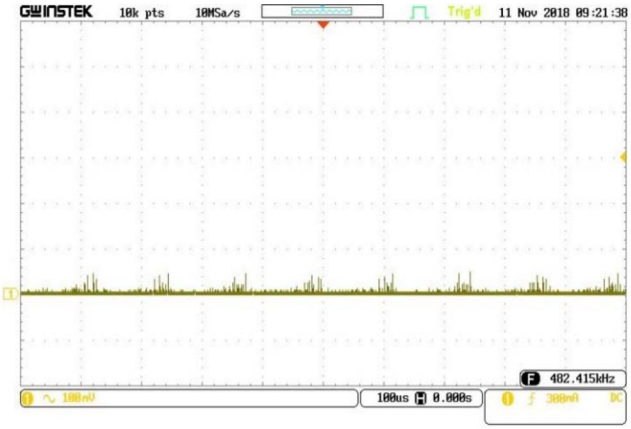

Fig. 29 *Experimental validation of the harmonic speed waveform of the FLC model*

7 Conclusion

When IM operates in less than full load condition, it can consume more power than needed. This excess power is in the form of heat. By using the FLC the starting current amplitude can be controlled and more power can be saved during this time. The inputs of the fuzzy controller are the error of speed and change of error which are used in the outer loop for producing an equivalent controller term. In this paper, a simulation study was conducted on a 50 hp IM-driven EV. Different performance indicators are tested such as peak overshoot, steady-state error, rise time, and settling time. The results showed that the phase current in the suggested system includes fewer loss components (less amplitude) with the same order components. The amplitudes of loss are reduced on the average for the actual torque in the steady state. It achieves a smooth torque and improves system performance. The simulation results of the suggested FLC scheme showed very good stability and better performance over the conventional PID controller in rising time, settling time, and peak overshoot. The proposed control system is validated by the experimental results which are in good agreement with the simulation results.

8 References

[1] Sato, E.: 'Permanent magnet synchronous motor drives for hybrid electric vehicles', *IEEJ Trans. Electr. Electron. Eng.*, 2007, **2**, (2), pp. 162–168

[2] Agency, I.E.: 'Global EV outlook 2016: beyond one million electric cars' (OECD Publishing)

[3] Sayed, K.: 'Zero-voltage soft-switching DC-DC converter-based charger for LV battery in hybrid electric vehicles', *IET Power Electron.*, 2019, **12**, (13), pp. 3389–3396

[4] Gomez, J.C., Morcos, M.M.: 'Impact of EV battery chargers on the power quality of distribution systems', *IEEE Power Eng. Rev.*, 2002, **22**, (10), pp. 63–63

[5] Stephan, C.H., Sullivan, J.: 'Environmental and energy implications of plug-in hybrid-electric vehicles', *Environ. Sci. Technol.*, 2008, **42**, (4), pp. 1185–1190

[6] Umetani, S., Fukushima, Y., Morita, H.: 'A linear programming based heuristic algorithm for charge and discharge scheduling of electric vehicles in a building energy management system', *Omega*, 2017, **67**, pp. 115–122

[7] Trovao, J.P.F., Roux, M.-A., Menard, E., *et al.*: 'Energy and power-split management of dual energy storage system for a three-wheel electric vehicle', *IEEE Trans. Veh. Technol.*, 2017, **66**, (7), pp. 5540–5550

[8] Buyukdegirmenci, V.T., Bazzi, A.M., Krein, P.T.: 'Evaluation of induction and permanent-magnet synchronous machines using drive-cycle energy and loss minimization in traction applications', *IEEE Trans. Ind. Appl.*, 2014, **50**, (1), pp. 395–403

[9] Sarigiannidis, A.G., Beniakar, M.E., Kladas, A.G.: 'Fast adaptive evolutionary PM traction motor optimization based on electric vehicle drive cycle', *IEEE Trans. Veh. Technol.*, 2016, **66**, (7), pp. 5762–5774

[10] Wang, Q., Niu, S., Luo, X.: 'A novel hybrid dual-PM machine excited by AC with DC bias for electric vehicle propulsion', *IEEE Trans. Ind. Electron.*, 2017, **64**, (9), pp. 6908–6919

[11] Boukadida, S., Gdaim, S., Mtiba, A.: 'Sensor fault detection and isolation based on artificial neural networks and fuzzy logic applicated on induction motor for electrical vehicle', *Int. J. Power Electron. Drive Syst.*, 2017, **8**, (2), pp. 601–611

[12] Varghese, S.T., Rajagopal, K.R.: 'Economic and efficient induction motor controller for electric vehicle using improved scalar algorithm'. IEEE 1st Int. Conf. on Power Electronics, Intelligent Control and Energy Systems (ICPEICES), Delhi, 2016, pp. 1–7

[13] Ulu, C., Korman, O., Komurgoz, G.: 'Electromagnetic and thermal analysis/design of an induction motor for electric vehicles'. The 8th Int. Conf. on Mechanical and Aerospace Engineering (ICMAE), Prague, 2017, pp. 6–10

[14] Ouchatti, A., Abbou, A., Akherraz, M., *et al.*: 'Sensorless direct torque control of induction motor using fuzzy logic controller applied to electric vehicle'. Int. Renewable and Sustainable Energy Conf. (IRSEC), Ouarzazate, 2014, pp. 366–372

[15] Makrygiorgou, J.J., Alexandridis, A.T.: 'Induction machine driven electric vehicles based on fuzzy logic controllers'. The 42nd Annual Conf. of the IEEE Industrial Electronics Society, Florence, 2016, pp. 184–189

[16] Li, H., Klontz, K.W.: 'Rotor design to reduce secondary winding harmonic loss for induction motor in hybrid electric vehicle application'. IEEE Energy Conversion Congress and Exposition (ECCE), Milwaukee, WI, 2016, pp. 1–6

[17] Kumar, R., Das, S., Chattopadhyay, A.K.: 'Comparative assessment of two different model reference adaptive system schemes for speed-sensorless control of induction motor drives', *IET Electr. Power Appl.*, 2016, **10**, (2), pp. 141–154

[18] Saleeb, H., Sayed, K., Kassem, A., *et al.*: 'Power management strategy for battery electric vehicles', *IET Electr. Syst. Transp.*, 2019, **9**, (2), pp. 65–74

[19] Das, S., Pal, A., Manohar, M.: 'Adaptive quadratic interpolation for loss minimization of direct torque controlled induction motor driven electric vehicle'. IEEE 15th Int. Conf. on Industrial Informatics (INDIN), Emden, 2017, pp. 641–646

[20] Sayed, K., Abo-Khalil, A.G., Alghamdi, A.S.: 'Optimum resilient operation and control dc microgrid based electric vehicles charging station powered by renewable energy sources', *Energies*, 2019, **12**, (22), p. 4240

[21] Sayed, K., El-Zohri, E., Naguib, F., *et al.*: 'Performance evaluations of interleaved ZCS boost DC-DC converters using quasi-resonant switch blocks for PV interface', *IOSR J. Electr. Electron. Eng., (IOSR-JEEE)*, 2015, **10**, (4), pp. 105–113

[22] Sayed, K., Gabbar, H.A.: 'Electric vehicle to power grid integration using three-phase three-level AC/DC converter and PI-fuzzy controller', *Energies*, 2016, **9**, p. 532

[23] Jasim, B.H., Dakhil, A.M.: 'New PI and PID tuning rules using simple analytical procedure'. The Second Scientific Engineering Conf., Mousil, Iraq, 2014

[24] Lin, W.-S., Huang, C.-L., Chuang, M.-K.: 'Hierarchical fuzzy control for autonomous navigation of wheeled robots', *IEE Proc., Control Theory Appl.*, 2005, **152**, (5), pp. 598–606

[25] Chan, C.: 'An overview of electric vehicle technology', *Proc. IEEE*, 1993, **81**, (9), pp. 1202–1213

[26] Wang, S.-C., Liu, Y.-H.: 'A modified PI-like fuzzy logic controller for switched reluctance motor drives', *IEEE Trans. Ind. Electron.*, 2011, **58**, (5), pp. 1812–1825

[27] Kalogirou, S.A.: 'Artificial intelligence for the modeling and control of combustion processes: a review', *Prog. Energy Combust. Sci.*, 2003, **29**, (6), pp. 515–566

[28] Mansour, M.F.: 'Design of an adaptive fuzzy controller through sliding mode concept'. PhD thesis, Faculty of Engineering, Mansoura University, 2005

[29] Panicker, D.K., Mol, M.R.: 'Hybrid PI-fuzzy controller for brushless DC motor speed control', *IOSR J. Electr. Electron. Eng. (IOSR-JEEE)*, 2013, **8**, (6), pp. 33–43

[30] Huang, H., Chang, L.: 'Continuous defuzzification of fuzzy logic controller in electric vehicle induction motor drives'. IEEE Int. Conf. on Systems, Man and Cybernetics. Intelligent Systems for the 21st Century, Vancouver, BC, Canada, 1995, vol. 3, pp. 2466–2471

[31] Shi, Y., Lorenz, R.D.: 'Induction machine design for dynamic loss minimization along driving cycles for traction applications'. IEEE Energy Conversion Congress and Exposition (ECCE), Cincinnati, OH, 2017, pp. 278–285

[32] Chrenko, D.: 'Influence of hybridization on eco-driving habits using realistic driving cycles', *IET Intell. Transp. Syst.*, 2015, **9**, (5), pp. 498–504

[33] Pal, A., Das, S.: 'A new sensorless speed estimation strategy for induction motor driven electric vehicle with energy optimization scheme'. IEEE 1st Int. Conf. on Power Electronics, Intelligent Control and Energy Systems (ICPEICES), Delhi, 2016, pp. 1–6

[34] Lee, B.-S., Krishnan, R.: 'Adaptive stator resistance compensator for high performance direct torque controlled induction motor drives'. Conf. Record of

1998 IEEE Industry Applications Conf. Thirty-Third IAS Annual Meeting (Cat. No.98CH36242), St. Louis, MO, USA, 1998, vol. 1, pp. 423–430
[35] Kunisetti, V.P.K., Meesala, R.E.K., Thippiripati, V.K.: 'Improvised predictive torque control strategy for an open end winding induction motor drive fed with four-level inversion using normalized weighted sum model', *IET Power Electron.*, 2018, **11**, (5), pp. 808–816
[36] Hu, J., Dawson, D.M, Qu, Z.: 'Adaptive tracking control of an induction motor with robustness to parametric uncertainty', *IEE Proc., Electr. Power Appl.*, 1994, **141**, (2), pp. 85–94
[37] Singh, M., Kumar, P., Kar, I.: 'Implementation of vehicle to grid infrastructure using fuzzy logic controller', *IEEE Trans. Smart Grid*, 2012, **3**, (1), pp. 565–577
[38] Sayed, K., El-Zohri, E., Mahfouz, H.: 'Analysis and design for interleaved ZCS buck DC-DC converter with low switching losses', *Int. J. Power Electron.*, 2017, **8**, (3), pp. 210–231
[39] Saleeb, H., Sayed, K., Kassem, A., *et al.*: 'Control and analysis of bidirectional interleaved hybrid converter with coupled inductors for electric vehicle applications', *Electr. Eng.*, 2019, **102**, (1), pp. 195–222. Available at https://doi.org/10.1007/s00202-019-00860-3

9 Appendix

9.1 Circuit parameters

See Table 5.

9.2 Controller parameters

See Table 6.

Table 5 Circuit parameters

Item	Parameters	Symbol	Value	Unit
battery	DC input voltage	V_i	780	V
inverter	snubber resistance	R_s	1000	Ω
	forward voltages	V_f	0.8	V
	switching frequency	F_{SW}	10	kHz
IM	nominal power	P_n	37.3	kVA
	voltage (line–line)	V_L	460	Vrms
	frequency	F_n	60	Hz
	number of poles	P	4	—
	mutual inductance	L_m	34.7	mH
	stator resistance	R_s	0.087	Ω
	rotor resistance	R_r	0.228	Ω
	stator and rotor leakage inductance	$L_{ls} = L'_{lr}$	0.8	mH
	moment of inertia	J	1.662	kg m^2
	rated speed	N	1780	rpm
	friction coefficient	F_c	0.1	N m s
	rated power	P_o	50	hp

Table 6 Controller parameters

	$k_p/k_1/Ge$	$k_i/k_2/Gde$	$k_d/k_3/Gu$
PID	5	30	1
FLC	1/120	2500	1